Smart Structures and Systems, *Vol. 32, No. 5 (2023) 319-338*
https://doi.org/10.12989/sss.2023.32.5.319

A vibration-based approach for detecting arch dam damage using RBF neural networks and Jaya algorithms

Ali Zar [1], Zahoor Hussain[*2,3], Muhammad Akbar [4], Bassam A. Tayeh [5] and Zhibin Lin[**2]

[1] *Key Lab of Structures Dynamic Behavior and Control of the Ministry of Education, Key Lab of Smart Prevention and Mitigation of Civil Engineering Disasters of the Ministry of Industry and Information Technology, Harbin Institute of Technology, Harbin 150090, China*
[2] *Department of Civil and Environmental Engineering, North Dakota State University, Fargo, ND 58018, USA*
[3] *Department of Civil Engineering, Sir Syed University of Engineering & Technology, Karchi 75300, Pakistan*
[4] *Department of Engineering Institute of Mountain Hazards and Environment, Chinese Academy of Sciences, Chengdu, China*
[5] *Civil Engineering Department, Faculty of Engineering, Islamic University of Gaza, P.O Box 108, Gaza Strip, Palestine*

(*Received January 30, 2023, Revised September 26, 2023, Accepted October 27, 2023*)

Abstract. The study presents a new hybrid data-driven method by combining radial basis functions neural networks (RBF-NN) with the Jaya algorithm (JA) to provide effective structural health monitoring of arch dams. The novelty of this approach lies in that only one user-defined parameter is required and thus can increase its effectiveness and efficiency, as compared to other machine learning techniques that often require processing a large amount of training and testing model parameters and hyper-parameters, with high time-consuming. This approach seeks rapid damage detection in arch dams under dynamic conditions, to prevent potential disasters, by utilizing the RBF-NNN to seamlessly integrate the dynamic elastic modulus (DEM) and modal parameters (such as natural frequency and mode shape) as damage indicators. To determine the dynamic characteristics of the arch dam, the JA sequentially optimizes an objective function rooted in vibration-based data sets. Two case studies of hyperbolic concrete arch dams were carefully designed using finite element simulation to demonstrate the effectiveness of the RBF-NN model, in conjunction with the Jaya algorithm. The testing results demonstrated that the proposed methods could exhibit significant computational time-savings, while effectively detecting damage in arch dam structures with complex nonlinearities. Furthermore, despite training data contaminated with a high level of noise, the RBF-NN and JA fusion remained the robustness, with high accuracy.

Keywords: arch dam; damage detection; jaya algorithm; neural network; radial basis function

1. Introduction

Economic development, agriculture, and power generation can all be supported by concrete dams. In the near future, these assets will no longer be useful due to premature damage (Dong and Catbas 2021). Replacement of Infra-structure is costly, laborsome. Consequently, engineers have created a number of methods to increase the structural integrity and safety of these buildings as well as lower the risk of both monetary and human losses. In recent times, the security problems of structures have gotten a lot of attention, and how to go about monitoring and assessing the status of large-scale structures has become a research topic. Structural features such as dynamic elastic modulus and stiffness will change once the structure is damaged, and result changes in structural dynamic response. Modal properties reflect the overall dynamic performance of the structure, and sensitive to dynamic behavior of structure (Chen and Ni 2018, Kang *et al*. 2017).

Dam parameters can be determined employing a promising method i.e., inverse analysis. Based on experimental data and model responses, inverse analysis aims at identifying input parameters that reduce deviations (Chen *et al*. 2019). Using the inverse sensitivity method, (Liu *et al*. 2017) assessed parameter instability of an unknown system. A method of inverse analysis was introduced by Bocciarelli and Ranzi (2018) for evaluating the hygrothermochemical parameters of concrete models. Inverse analysis was used by Vorel and Kabele (2019) to identify quasi-brittle solid failure modes. The mechanical properties of concrete dams were recently simulated through dynamic parameter inverse analysis (Kang *et al*. 2021). Vibration tests have been used to investigate dynamic inversion methods in recent years. It has been demonstrated that a variety of techniques, including natural frequencies, mode shapes, curvature mode forms, and techniques that combine mode shapes and frequencies, can be employed to identify vibration-based damage (Kang *et al*. 2021, Majumdar *et al*. 2012, Nhamage *et al*. 2016). Wang *et al*. (2012) used a back analysis to research the seismic response of dams. Modal parameters are retrieved from model parameters, and they are independent of the stimulation given to the structures (Majumdar *et al*. 2012). This study uses vibrational modal data to calculate the

*Corresponding author,
E-mail: dutian17@outlook.com;
zahoor.hussain@ndus.edu
**Co-corresponding author, Associate Professor,
E-mail: Zhibin.lin@ndus.edu

http://www.techno-press.org/?journal=sss&subpage=7
ISSN: 1738-1584 (Print), 1738-1991 (Online)

DEM and degree of damage in arch dam.

Due to the combination of several factors in a sizable search space, inverse dynamic analysis necessitates the employment of a global optimization technique. A proper goal function that is coupled to structural parameters is required to identify the parameter value that is most appropriate (Nguyen-Tuan *et al*. 2018). Particle swarm optimization (PSO) and genetic algorithms (GA) were used by Khatir *et al*. (2017) to successfully identify graphite-epoxy composite beams. According to Kang *et al*. (2016), PSO and least-square support vector machine (LS-SVM) were used to determine slope stability and other researchers also used it for prediction performance (Deng *et al*. 2019, Yuan *et al*. 2019). Yang *et al*. (2019) used enhanced PSO to determine elastic moduli of dam body and foundation. Using JA, a novel global optimization method, does not need changing any variables related to the algorithm (Kaveh and Laknejadi 2013, Rao and More 2017). In their combined technique for inverting dynamic parameters in concrete dams, Kang *et al*. (2021) recommended the use of Gaussian process regression (GPR) with Jaya optimization. Therefore, this work employs JA for vibration response-based inverse analysis to discover faults by minimising the objective function.

Different stochastic, statistical, and hybrid mathematical models have been created to forecast dam structural behaviour based on physical principles (Stojanovic *et al*. 2013, Teng *et al*. 2023). When studying uncommon or unorthodox situations, FEMs are more adaptable. The aforementioned models are useful since early in a structure's lifespan there isn't enough data to create database predictive models. When utilising these techniques, a variety of geometry- and boundary-related assumptions and simplifications are made, which might result in mistakes in material characterisation. There is a requirement for a big finite element model (FE) for infra-strcuture modelling. The iterative parameter inversion approach involves a substantial number of finite element calculations, which substantially raises calculation cost. In order to speed up the calculation of an inverse analysis, a surrogate model can be utilised in place of a full FE model (Lew *et al*. 2006, Zhang *et al*. 2020).

Deep learning, multiple regression analysis, and machine learning are clever methods for examining civil infrastructure model data (Tsihrintzis *et al*. 2019). Artificial intelligence techniques in the structure health monitoring field include support vector machines, artificial neural networks (Kohiyama *et al*. 2020, Le and Caracoglia 2020), gaussian surrogate models (Kang *et al*. 2021), and kernel regression techniques (Lederman *et al*. 2014). The techniques need little starting data and are computationally efficient. Swarm intelligence approaches may be used with machine-learning-based swarm intelligence techniques to increase optimization performance limitations and get over damage detection uncertainties (Pandit *et al*. 2018). An artificial neural network can recognize patterns, diagnose damage, automate control, and be applied in a variety of other areas (Kang *et al*. 2017). Neural networks can perform nonlinear mappings to filter out noise and perform correct identification in noisy scenarios, making them particularly useful for nonlinear pattern recognition and classification. The network input vector consists of structural damage-sensitive parameters, the output vector consists of structural damage states, and the training sample set is compiled by extracting features from the structure's response. Once trained, the neural network has the ability to classify patterns based on input parameters and damage states. In the following step, the structure's dynamic parameters are measured and networked, and damage status information is obtained (Deng *et al*. 2019, Taheri *et al*. 2020). Once the training process has been completed, the calculation application will become faster. Therefore, neural networks are capable of explaining structural changes as well as reflecting the extent of structural damage (Dou *et al*. 2019, Rajasekaran and Amalraj 2002, Zhang and Zhang 2004).

Herein, For the purpose of damage identification utilising RBF and JA, an investigation of the vibration response of a concrete arch dam using dynamic parameter inversion is presented. To gather pseudo-experimental data, forward FE analysis was performed by adding mass to the arch dam and adjusting various material characteristics. To make the most of regression analysis and global optimization techniques, RBFs were used as a stand-in model for the FE model. It was connected to PSO-based objective function optimization, Genatic algorithm and JA-based objective function optimization to proposed the best possible combination.

This paper is structured as follows: A technique for damage detection based on vibration responses is discussed in Section 2. Materials for damage detection are included in the RBF-driven optimization process, as detailed in Section 3. Numerical outcomes are presented in Section 4. In Section 5, conclusions are provided.

2. Research significance

Our research focuses on simplifying damage detection strategies in complex infrastructure structures such as arch dams, addressing gaps in existing methods such as computational intensity, multiple user defined parameters and real-time monitoring challenges. Our novel combination of RBF neural networks and the Jaya algorithm yields a model with only one user-defined parameter, σ, reducing variability sources and streamlining the tuning process. Because of the complexities of DNN-based methods' architecture like layer's depth, neuron count, activation function, batch size and other essentially parameters (Samaniego *et al*. 2020, Nanthakumar *et al*. 2016), our model minimizes these risks. Traditional approaches (Anitescu *et al*. 2019), while scientifically sound, may not be suitable for continuous monitoring of highly non-linear structures due to computational demands in real time monitoring. Our model combines scientific rigor with practical applicability, giving it a distinct advantage in the damage detection domain. Considering the conventional mechanisms of structural health monitoring of concrete structures (Abbas *et al*. 2022, Ahmed *et al*. 2021, Hussain *et al*. 2021) this study used the RBF neural network

because of its high predictive ability in detecting concrete arch dam damage. Moreover, compared to other machine learning and deep learning methods, the propsed novel hybrid approach use only one user defined parameter i.e NSR component that makes it more generalizeable and reliable for real-world problems, where limited collected data could make powerful deep learning invalid.

3. A vibration-based method for detecting damage to arch dams

3.1 Parameterization of arch dam damage

An intact structural system is characterized by its modal characteristics using the eigenvalue formula

$$\boldsymbol{K}\phi_i - \omega_i^2(\boldsymbol{M_D} + \boldsymbol{M}_P)\phi_i = 0 \tag{1}$$

A dam's structural stiffness matrix is **K**, structural mass matrix $\mathbf{M}_D$, added mass matrix $\mathbf{M}_P$ represents the dam and the reservoir dynamic interaction, ω_i is *i*th frequency, and ϕ_i the mode shape. Added mass of water in a reservoir The additional mass formula by Westergaard may be used to compute M*i* (Pan *et al*. 2015)

$$M_i = \frac{7}{8}\rho_o A_i\sqrt{Hh_i} \tag{2}$$

where, a node is defined by its added mass M_i, density ρ_o, surface area M_i, water depth H, and node distance h_i from the surface of the water. In Fig. 1, the upstream surface of the arch dam elements is shown with mass added.

The dam's unknown statistical and physical properties serve as updated parameters. Most practical applications assume there is no transition between mass damage and the preceding state. Thus, the damage index d_e was used to parameterize the element properties. According to continuum damage dynamics (Contursi *et al*. 1998), damage effects can be assessed by scalar factors ranging from 0 to 1. The dam will be perfectly fine if its value is 0, while it will be fractured if its value is approximately 1. Damage is the concept for a decrease in the stiffness of discretized finite elements, as seen here

$$k_d^e = k^e(1 - d_e) \tag{3}$$

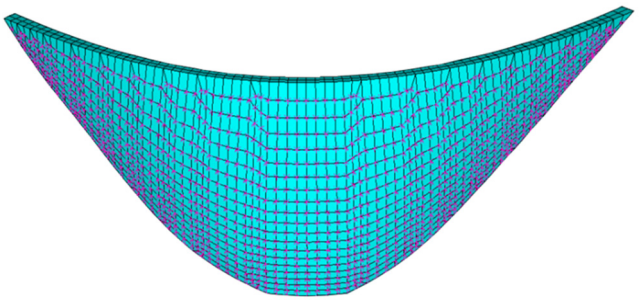

Fig. 1 Mass added to arch dam surface nodes upstream

For the system's *e*th element, k^e and k_d^e represent the intact stiffness matrix for that element and d_e represents the damage index for that element. This concept of estimation of damage magnitude and position, both at the level of the element, allows the identification of damage at the element level (Perera and Ruiz 2008).

3.2 Damage detection objective function composed on vibration data

During structural changes, natural frequencies and mode shapes fluctuate, which is fundamental to hydraulic structures. Accordingly, vibration responses can be used to detect damage (Alkayem *et al*. 2018).

3.2.1 Frequency based objective function

It is possible to express the natural frequency in the following manner

$$\Omega R = \gamma_i \sum_{i=1}^{nf} \left(\frac{f_i^m - f_i^c(\boldsymbol{E})}{f_i^m}\right)^2 \tag{4}$$

FE models of undamaged and damaged structures yield, f_i^m and f_i^c natural frequencies, correspondingly; γ represents the weighting factor for output error in frequency change objective function, **E** represents vector of parameters to optimize; *nf* represents the number of frequencies.

3.3 Utilizing both mode shapes and frequencies to derive an objective function

The coordinate model assurance criteria (COMAC) is used to pinpoint the location and size of the structural fault. A scalar constant that represents the degree of precision between two reference modal vectors is as follows

$$COMAC(m,c) = \frac{(\sum_{i=1}^{nm}\phi_i^m\,\phi_i^c(\boldsymbol{E}))^2}{(\sum_{i=1}^{nm}\phi_i^m\,\phi_i^m)(\sum_{i=1}^{nm}\phi_i^c\,\phi_i^c)} \tag{5}$$

The modal components in the real FE models of the unharmed and damaged buildings are designated by ϕ_i^m and ϕ_i^c, respectively, and *nm* represents the number of modes. The COMAC level, which has a scale from 0 to 1, represents how similar distinct pairs of modal vectors are to one another, ranging from entirely uncorrelated to perfectly correlated. The COMAC value of approximately 0 indicates a possible damage position (Khatir *et al*. 2017). A weighting factor β based on the output error of the objective function can be determined by *n* times the measured mode numbers. Eqs. (4) and (5) therefore describe the objective function, that depends on combination of natural frequency and mode shape changes.

$$\begin{aligned} f = \gamma \sum_{i=1}^{n}\left(\frac{f_i^m - f_i^c(\boldsymbol{E})}{f_i^m}\right)^2 \\ +\beta \sum_{i=1}^{n}\{1 - COMAC[\phi_i^m, \phi_i^c(\boldsymbol{E})]\} \end{aligned} \tag{6}$$

where γ and β are less than unity; $\gamma + \beta = 1.0$. In this

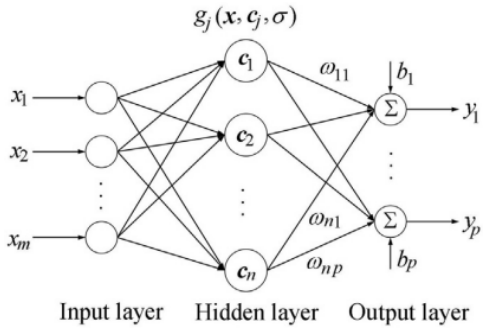

Fig. 2 The structure of RBF neural networks (Dou *et al*. 2019)

researchwork, both γ and β are equal to 0.5 (Kang *et al.* 2021).

4. An intelligent optimization algorithm (RBF neural networks) based damage identification

4.1 RBF

A RBF network consists of three layers: input, hidden, and output. RBF network structure is shown in Fig. 2. Input layer neurons are equal to problem dimensions $x = [x_1, x_2, x_3, \ldots, x_m]^T$. A hidden layer function $g = [g_1, g_2, g_3, \ldots, g_j, \ldots, g_n]^T$ processes data in the input layer. $y = [y_1, y_2, y_3, \ldots, y_p]^T$ is produced by summing the data seen in hidden layer and sending it to output layer (Rajasekaran and Amalraj 2002, Zhang and Zhang 2004).

$$\begin{cases} y = \omega^T g + b \\ g_j(x, c_j, \sigma) = exp\left[-\|x - c_j\|^2/(2\sigma^2)\right] \end{cases} \quad (7)$$

$\|x - c_j\|^2$ is the Euclidean distance between x and c_j that determines neuronal sensitivity σ, where c_j is one of a group of center vectors with the same size as x. The network weight vector for output neurons is $\omega = (\omega_{jk})_{n\times p}$, and the output neurons' offset matrix is $b = [b_1, b_2, b_3, \ldots, b]^T$.

In the literature, it has been documented that, with sufficient neurons and training data, an RBF network is capable of approaching any nonlinear function (Rajasekaran and Amalraj 2002, Zhang and Zhang 2004). The RBF-based surrogate model is constructed via training neural networks. Two classes of existing information data are needed in order to create the RBF model. Latin hypercube sampling is used to create the data sets for surrogate model, which is produced using random sampling to build the mapping connection. Different data sets are utilised for training and testing this model (Olsson *et al.* 2003, Trinh and Jun 2021). In order to assure authenticity and validate of the RBF-based surrogate model, its neural sensitivity regulator (NSR) component i.e., σ was exploared first. Usually, the neural sensitivity regulator operates within a range between 1 and 10.

4.2 Jaya algorithm

Rao (2016) put out the Jaya algorithm as a population-based approach to global optimization. The method basically assumes that any population solution will always move away from the least desired option and toward the most ideal one. This method has the benefit of simply requiring a single equation and not requiring tuning algorithm-specific limitations. Hence, it is simple to comprehend (Rao and More 2017) and distinguishes itself from other metaheuristic neural networks. Jaya's algorithm is represented mathematically as follows.

In this case, let $f(\boldsymbol{u})$ be the optimized objective function. In the initial problem space, m solutions $\{\boldsymbol{u}_1, \boldsymbol{u}_2, \ldots, \boldsymbol{u}_m\}$ are randomly generated. In addition to analyzing these initial solutions, $\boldsymbol{u}_{best}$ and $\boldsymbol{u}_{worst}$ are determined by the objective function. These solutions then perform search loop by loop until the maximum generation threshold is reached. Each time an iteration is performed, the population solution is customized as shown in the equation

$$\begin{aligned} \boldsymbol{v}_{j,k} = \boldsymbol{u}_{j,k} + r_{1,j}\left(\boldsymbol{u}_{j,best} - \left|\boldsymbol{u}_{j,k}\right|\right) \\ -r_{2,j}\left(\boldsymbol{u}_{j,worst} - \left|\boldsymbol{u}_{j,k}\right|\right) \end{aligned} \quad (8)$$

In this equation, $\boldsymbol{u}_{j,best}$ indicates the value of variable j for the best candidate, $\boldsymbol{u}_{j,worst}$ indicates the value of variable j for the worst candidate, and $\boldsymbol{v}_{j,k}$ represents $\boldsymbol{u}_{j,k}$ modified, while $r_{1,j}$ and $r_{2,j}$ represent two arbitrary constants between [0, 1] in each cycle. Solution $r_{1,j}(\mathbf{u}_{j,best} - |\mathbf{u}_{(j,k)}|)$ represents the solution's ability to move closer to the best solution, while solution $r_{2,j}(\mathbf{u}_{j,best} - |\mathbf{u}_{(j,k)}|)$ represents the solution's ability to prevent the worst solution. There is a thorough search of the search space due to the arbitrary constants r_1 and r_2. By increasing the absolute value of the solution space $|\mathbf{u}_{(j,k)}|$, the algorithm's search capacity is further enhanced. Newly generated candidate solutions will be analyzed using the objective function. Replacement of the old solution is recommended if it is better than the new one, otherwise, leave it unchanges. A better fitness value is assigned to $\boldsymbol{v}_{(j,k)}$ if it gives a better fitness value. Following each iteration, all accepted solutions are saved and utilized in the searches for

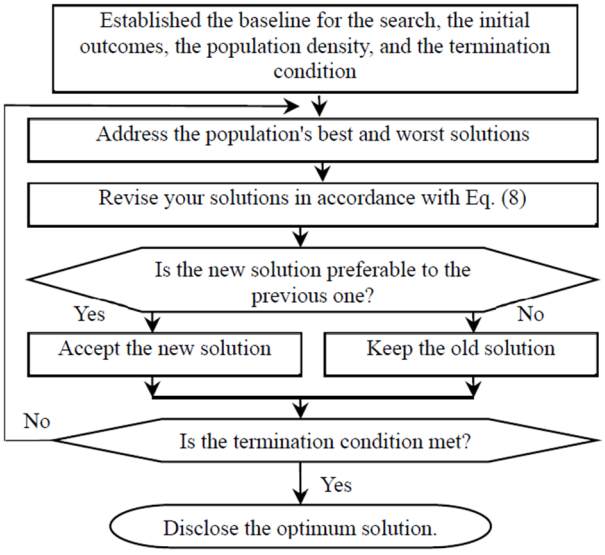

Fig. 3 A flow chart illustrating the Jaya algorithm (Rao and More 2017)

the following iteration. The best solution to a problem is found using the suggested algorithm, and the poorest option is rejected. As shown in Fig. 3, the Jaya algorithm is schematically represented.

4.3 Parameter selection and validation for RBF surrogate model

The best value of neural sensitivity regulator component i.e., σ will be adjusted to a certain level, which will give least value of mean square error (*MSE*) for generated surrogate model, using Eq. (9). The σ is checked in a range [1.0, 10] as its value should not be equal to zero, for RBF neural network. The best value will be used to construct RBF based surrogate model.

$$MSE = \left[\frac{1}{N_m}\sum_{i=1}^{N_m}(y_{Dm}(i) - (y_m(i))^2 + \frac{1}{N_f}\sum_{i=1}^{N_f}(y_{Df}(i) - (y_f(i))^2\right] \quad (9)$$

Where y_{D_f} and y_{Dm} specify the individual simulated frequency and mode shapes, respectively; y_f and y_m denote individual measured frequency and mode shapes. N_f and N_m represents the set of observations for frequency and mode shapes. The mean absolute error (*MAE*), root mean square error (*RMSE*), and correlation coefficient (*R*) are also utilized to validate the best surrogate model.

$$MAE = \frac{1}{N}\sum_{i=1}^{N}|y_D(i) - y(i)| \quad (10)$$

$$RMSE = \sqrt{\frac{1}{N}\sum_{i=1}^{N}(y_D(i) - y(i))^2} \quad (11)$$

$$R = \frac{[\sum_{i=1}^{N}(y_D(i) - \overline{y_D})\,(y(i) - \bar{y})]}{(\sum_{i=1}^{N}(y_D(i) - \overline{y_D}))(\sum_{i=1}^{N}(y(i) - \bar{y}))} \quad (12)$$

A simulated value y_D is an individual value; an average value $\overline{y_D}$ is an average of many simulated values; y is measured value; $\bar{y}$ is an individual value; *N* is the set of measurements. Models with *MAE* and *RMSE* of approximately zero, as well as *R* of approximately one, are considered the best.

4.4 Damage identification procedure based on RBF surrogate models and intelligent optimization

Multi-parameter detection of high arch dam damage is performed using the following steps.

Step 1: Identify the problem. Estimate the DEM using Equation 3 by assuming a damage percentage in the dam components. In order to simulate the natural frequencies and mode shapes measured, forward FE analysis results are used.

Step 2: Establishing sample points. Latin hypercubic sampling (LHS) concept is used to generate training and test sample points (Olsson *et al*. 2003, Trinh and Jun 2021). It ensures that the entire range of each variable is represented in the sampled data, thereby potentially enhancing the quality of the data used to train and test the model. Moreover, Training samples accounted for about 80% of the selected data, and test samples accounted for about 20% of the selected data (Goodfellow *et al*. 2016).

Step 3: Create training datasets. It consists of modal parameters and sample points. Apply the FE model to sample points in order to calculate the modal parameters.

Step 4: Create a surrogate RBF model using training data. Use the test set and assure the accuracy of established RBF model. Repeat process from Step 3, tune the NSR component or create further sample points if surrogate model's sensitivity is insufficient to satisfy the requirements.

Step 5: Apply the Jaya to minimize the objective function. Analyze inversely the dam parameters to predict damage. In order to obtain natural frequencies and mode shapes, replace the FE model with the RBF surrogate model.

Step 6: calculating or obtaining the DEM values.

The proposed approach is shown in Fig. 4.

5. Numerical cases for damage detection

5.1 Foundation properties and boundary conditions for arch dam

With 480-meter-long arches and 240-meter-high dams, arch dams feature parabolic hyperbolic forms. An illustration of the different radii of the arch rings is shown

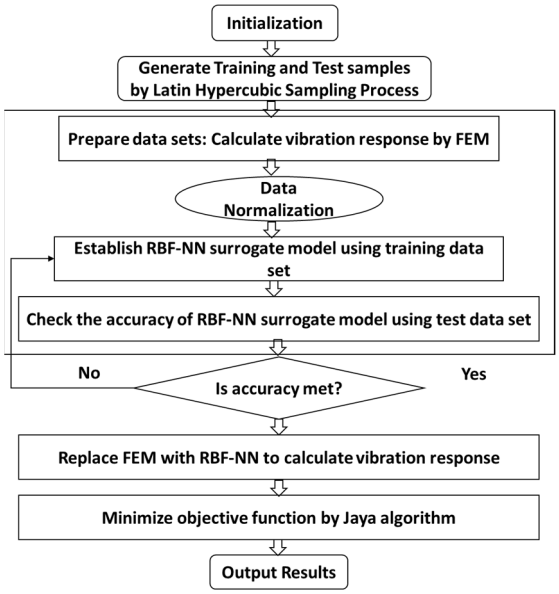

Fig. 4 Overview of the proposed techniques for the detection of damage in arch dams based on vibration responses and a surrogate model based on RBF

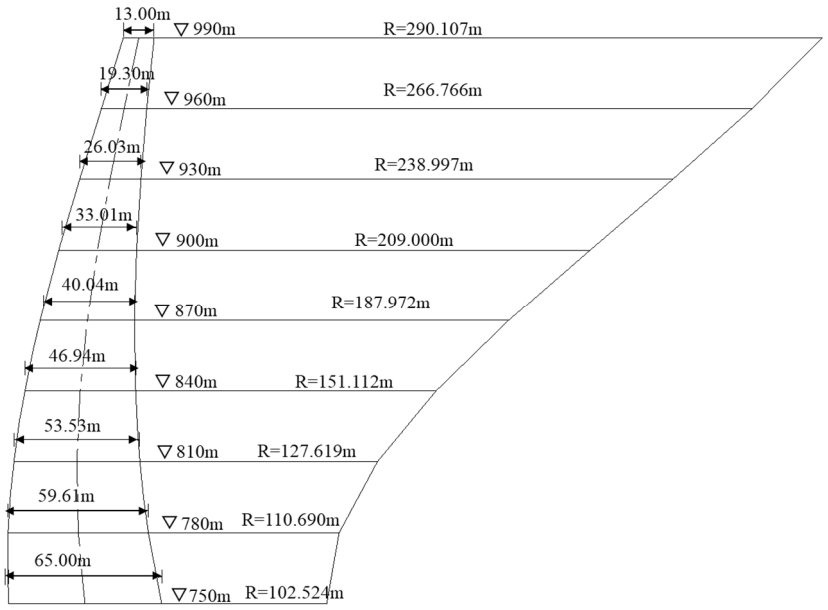

Fig. 5 Section view of a hyperbolic parabolic arch dam (arch ring radius is indicated by the letter R)

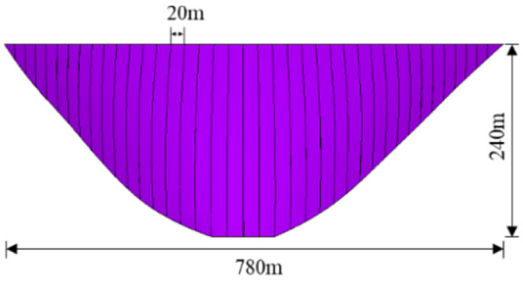

Fig. 6 A front view of a vertically joint arch dam

in Fig. 5 in a sectional view of the arch crown beam.

Each vertical joint in Fig. 6 is spaced 20 metres apart. According to Fig. 1, the dynamic impacts of a dam were calculated to be half of the Westergaard added mass, up to 971 meters in height.

The foundation rock masses in the left, right, and downward directions are denoted by F1, F2, and F3, respectively, as shown in Fig. 7(a), and their DEMs were 30, 28, and 25 GPa, respectively in both cases, which will be discussed in the following sections. The Poisson ratios

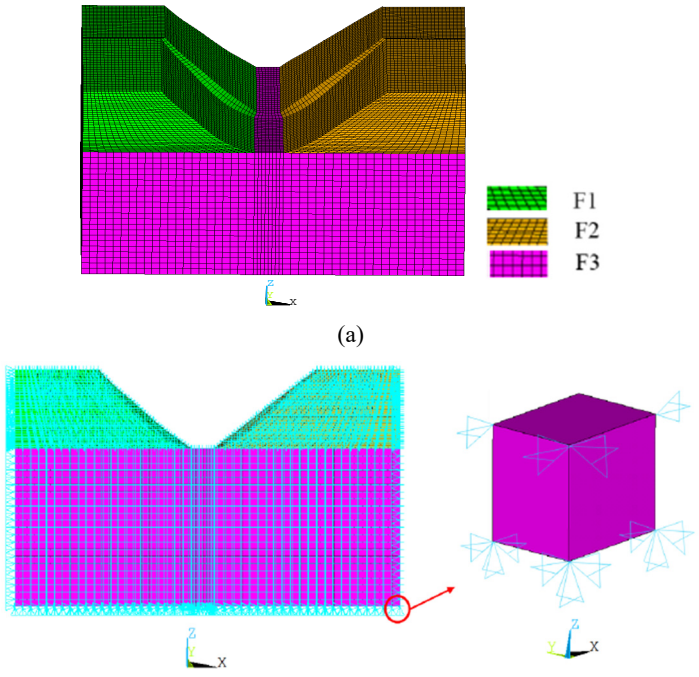

(a)

(b)

Fig. 7 Arch dam foundation: (a) foundation classification w.r.t DEMs; (b) foundation constrained boundary

Table 1 Limits and constants defined in optimization algorithms

User defined limits	Jaya	PSO	GA
Number of runs (run)	30	30	30
Number of iterations (maxGen)	1000	1000	1000
Size of population (sizepop)	50	50	50
Lower boundary (lb)	0.5	0.5	0.5
Upper boundary (ub)	1.5	1.5	1.5
User defined constants			
c_1	-	2.0	-
c_2	-	2.0	-
Number of chromosomes (N_c)	-	-	20.0
Crossover rate (P_c)	-	-	0.95
Mutation probability (P_m)	-	-	0.001
Elite rate (E_r)	-	-	0.20

for each dam and foundation component were 0.17 and 0.25, respectively. The density of the dam material for each component was 2400 kg/m^3. We assumed that damage occurred in the dam body but the foundation remained intact, and that the foundation was a massless foundation. All the outer surface nodes of the foundation and side rock mass were constrained in the x-, y-, and z-axis directions, as shown in Fig. 7(b).

5.2 Limits and constants defined in optimization algorithms

The iteration limits and number of runs are important characteristics that influence on the performance and end results of optimization algorithms. Furthermore, each meta-heuristic optimization algorithm has its own fundamental parameters that may affect its search operation. So, it is quite important to set iteration limits and constants values, defined in an algorithm for its better performance. Table 1 shows such kind of data that was set for the algorithms investigated in this study. The computation was performed using MATLAB R2020a and ANSYS 18.1 Mechanical for FE analysis, on a computer with an Intel(R) Core (TM) i7-9700F CPU @ 3.00 GHz.

Table 2 Material properties of arch dam in Case A

Arch dam part	Actual DEM (MPa)	Assumed damage index (d_e)	Measured DEM (MPa)
D1	36000	15%	30600
D2	34000	18%	27880
D3	37000	0%	37000
D4	48000	10%	34200
D5	41000	20%	32800

The improved PSO, and elitist preservation-strategy-based GA are three excellent intelligent optimization algorithms that are comparable to the Jaya optimizer. For PSO and GA, the user defined constants were set based on Kang *et al*. (2016) and Mirjalili (2023), respectively. Each algorithm was performed 30 times independently, and then the average values were adopted to avoid the randomness and escape from local optima.

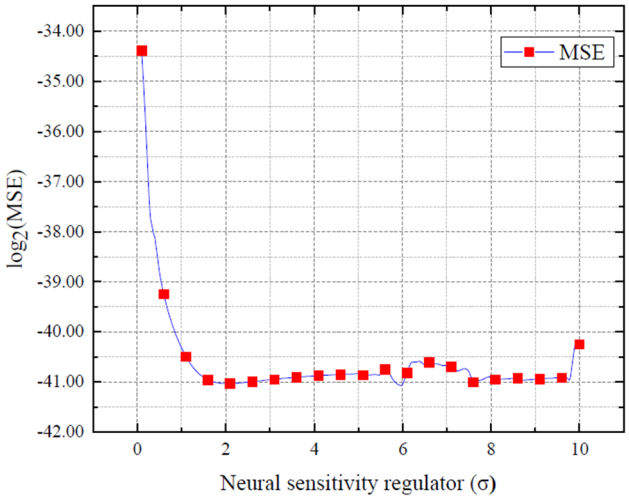

Fig. 9 The effect of neural sensitivity regulator i.e., σ on MSE for surrogate model in case A

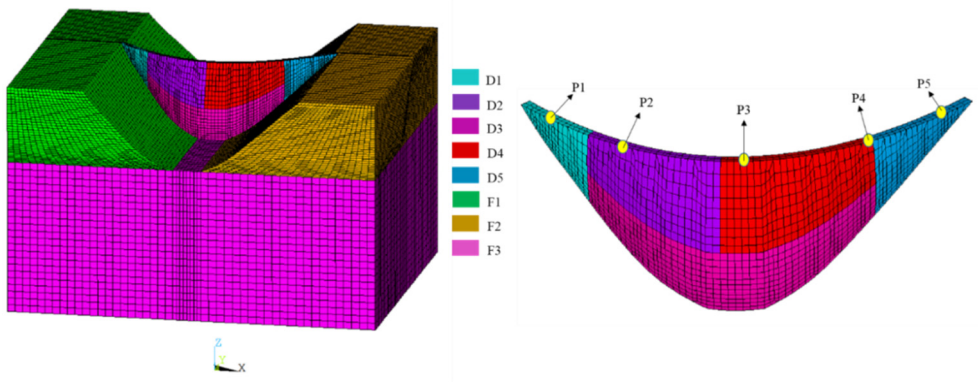

(a) (b)

Fig. 8 Arch dam–foundation system for Case A with DEM boundaries: (a) arch dam–foundation system; (b) selected nodes on arch dam crest surface

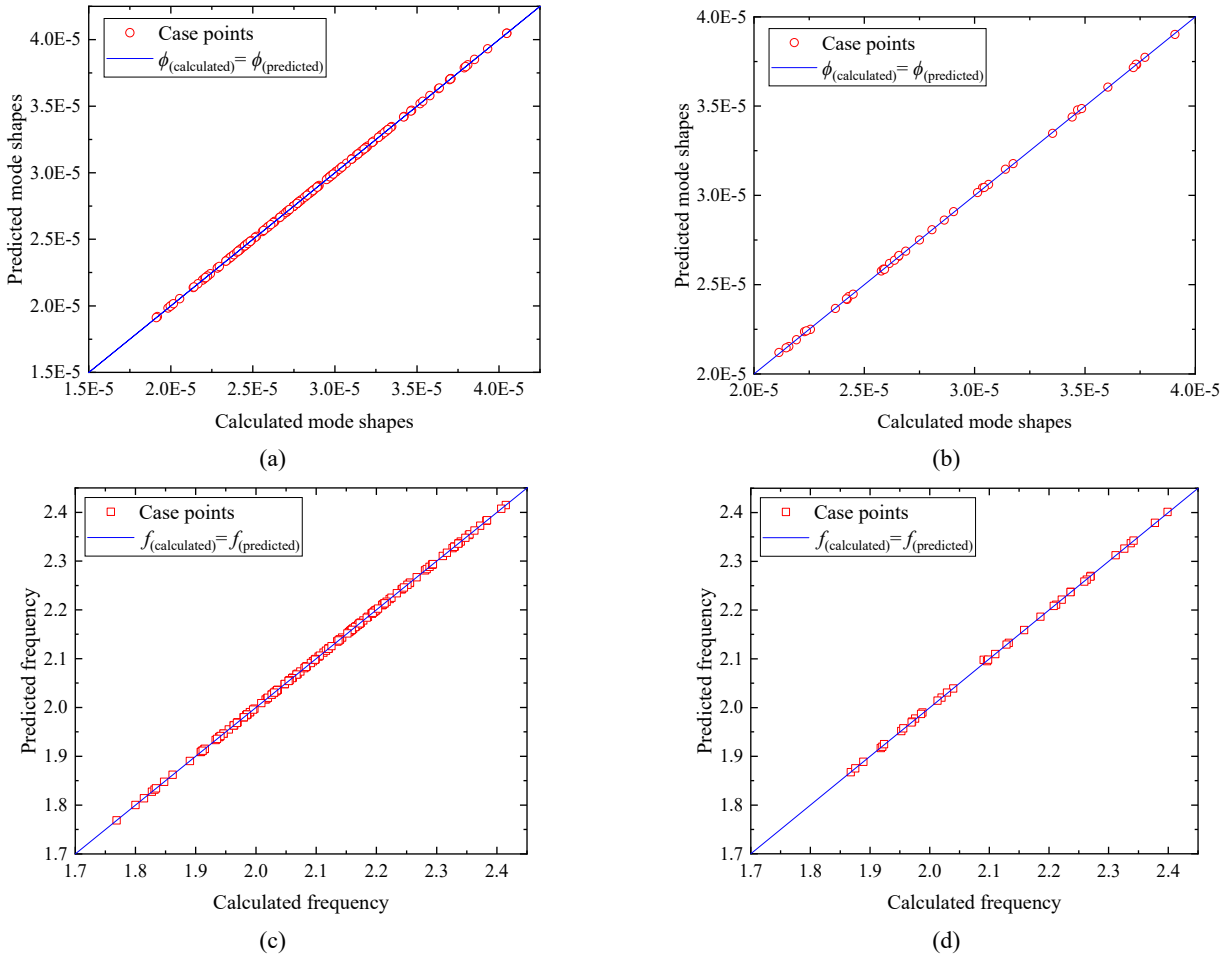

Fig. 10 Comparison between modal parameters calculated using FEM and predicted by RBF model in Case A for mode shapes and frequencies: (a), (b) Training datasets; (c), (d) Test datasets

5.3 Numerical case A

5.3.1 Description of arch dam properties for case A

In Case A, the arch dam body was classified into five different sections. The assumed properties of the dam are listed in Table 2, and a visual illustration is shown in Fig. 8(a). To calculate the frequency and mode shapes, a layout scheme of the measurement points is provided in Fig. 8(b).

5.3.2 Selection of neural sensitivity regulator component for case A

The neural sensitivity regulator component i.e., σ is selected equal to 5.9. The effect of σ on RBF based surrogate model is shown in Fig. 9.

Table 3 Fitting accuracy of RBF-based surrogate model in Case A

Data type	Natural frequency			Mode shapes		
	MAE	RMSE	R	MAE	RMSE	R
Training data	4.34E-10	9.32E-10	1.000	1.73E-07	6.89E-07	0.999
Test data	3.06E-08	4.76E-08	1.000	3.58E-06	9.24E-06	0.975

5.3.3 RBF based surrogate model for case A

Fig. 10 shows the correlation between mode shapes and frequencies calculated with the FEM and predicted by the RBF model. As shown, all sample points were distributed near the diagonal, implying that the RBF model predicted the same vibration responses as the FE results. The RBF model's fitting accuracy is listed in Table 3.

5.3.4 Damage identification process by RBF for case A

Fig. 11 depicts the evolution of the objective function values for the three algorithms. The numerical values of the PSO algorithm and Jaya algorithm converged at 1.12E-04 and 1.14E-04, respectively, whereas the numerical value of the GA algorithm converged at 2.09E-04, as shown in Fig. 11(a). The measured real frequencies and mode shapes were each subjected to 1% and 10% noise, respectively, to further confirm the fineness operation of the algorithms. Although noise was introduced, the PSO algorithm and Jaya algorithm converged at 6.82E-05 and 6.92E-05, respectively, whereas the GA provided the best solution at 1.90E-04, as shown in Fig. 11(b).

Fig. 12 (without noise) and Fig. 13 (with noise), depict the identification process for calculated damage indices d_1 and d_5 detected in dam parameters D1 and D5, respectively.

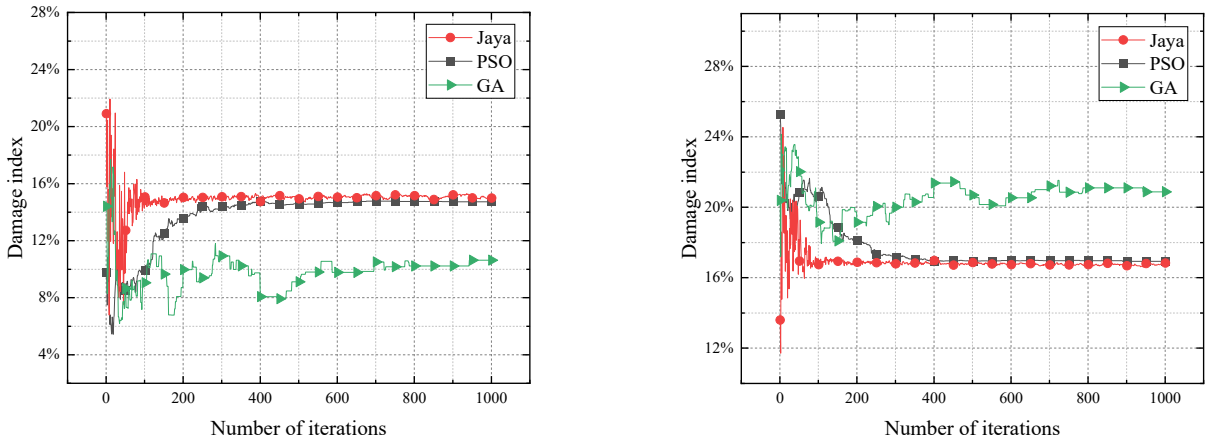

Fig. 12 Identification process of damage index of arch dam parameters without noise in Case A using RBF model: Damage index detected in (a) D1; and (b) D5

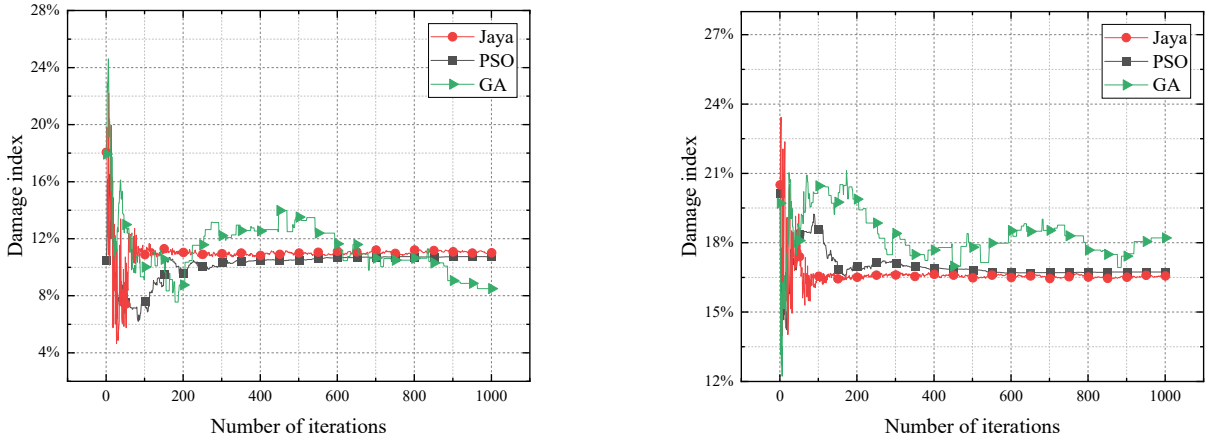

Fig. 13 Identification process of damage index of arch dam's parameters with noise in Case A using RBF model: Damage index detected (a) D1; and (b) D5

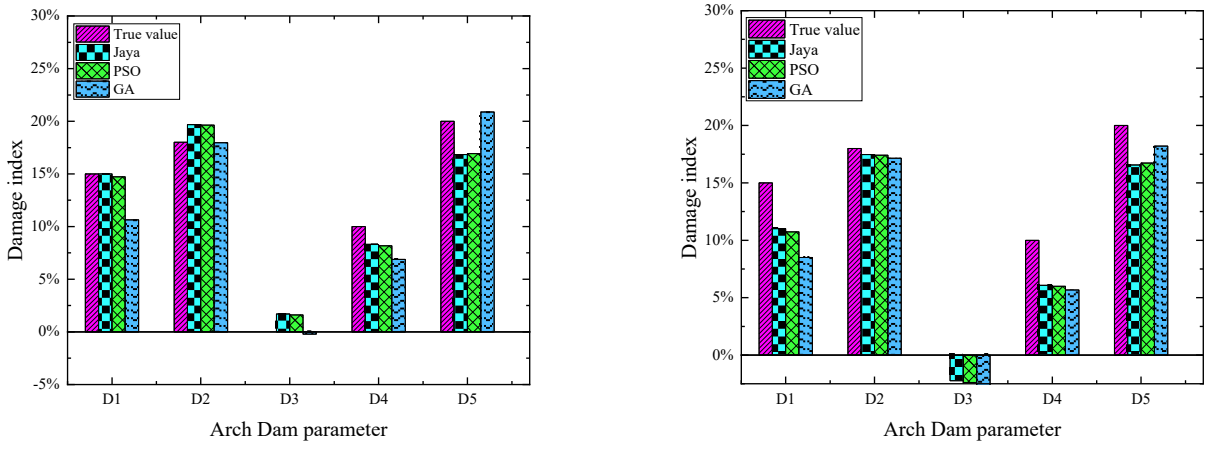

Fig. 14 Comparison between true and calculated damage index values for Case A using RBF: (a) Without noise; (b) with noise

Table 4 Comparison of measured and calculated DEM results, without noise for Case A with the RBF-based surrogate model

Arch dam part	Measured DEM (MPa)	Jaya		PSO		GA	
		Calculated value (MPa)	Relative error (%)	Calculated value (MPa)	Relative error (%)	Calculated value (MPa)	Relative error (%)
D1	30600	30602.169	0.007	30697.024	0.317	32171.081	5.134
D2	27880	27305.397	2.061	27322.493	2.000	27893.806	0.050
D3	37000	36370.709	1.701	36404.622	1.609	37077.003	0.208
D4	34200	34849.439	1.899	34892.273	2.024	35386.264	3.469
D5	32800	34097.412	3.956	34054.939	3.826	32438.808	1.101
Average of errors (%)			**1.925**		**1.955**		**1.992**
Time of 30 runs (s)		**140.117**		**144.149**		**320.007**	

Table 5 Comparison of measured and calculated DEM results, with noise for Case A with the RBF-based surrogate model

Arch dam part	Measured DEM (MPa)	Jaya		PSO		GA	
		Calculated value (MPa)	Relative error (%)	Calculated value (MPa)	Relative error (%)	Calculated value (MPa)	Relative error (%)
D1	30600	32034.871	4.689	32136.643	5.022	32938.032	7.641
D2	27880	28060.679	0.648	28080.499	0.719	28172.848	1.050
D3	37000	37826.379	2.233	37884.940	2.392	38316.181	3.557
D4	34200	35688.007	4.351	35723.746	4.455	35845.393	4.811
D5	32800	34208.153	4.293	34139.764	4.085	33533.318	2.236
Average of errors (%)			**3.243**		**3.335**		**3.859**
Time of 30 runs (s)		**142.211**		**144.258**		**326.630**	

The calculated values of d_1, d_2, d_3, d_4 and d_5 using Jaya were 14.99%, 19.69%, 1.70%, 78.29%, and 16.84%, respectively, which are similar to the assumed damage index, while the values after noise were 11.01%, 17.47%, -2.23%, 6.084%, and 16.56%, which are similar to the measured damage index without noise.Finally, in Fig. 14, the calculated damage index values for all parameters identified using the PSO algorithm, Jaya optimizer and GA are compared to verify the accuracy of our technique, both with and without noise. Among all the damage detection algorithms, the Jaya produced the lowest average relative errors. The Jaya produced average errors of 1.654% and 2.820% for damage index identification with and without noise, respectively.

5.3.5 DEM calculations by dynamic parameter inversion analysis for case A

In Case A, Tables 4 and 5 compare measured and calculated DEM results without and with noise using the PSO algorithm, Jaya algorithm and GA with the RBF-based surrogate model of the arch, respectively. The relative errors and their average values are presented to compare the accuracy of the results. In addition, the computing time is provided to compare the three algorithms' efficiencies. The results of the cases with and without noise were reasonable, and the Jaya outperformed the other algorithms in terms of speed and accuracy. The GA performed poorly in terms of parameter identification, with the average relative error of parameter identification being 1.723% without noise and 3.406% with noise.

5.4 Numerical case B

5.4.1 Description of arch dam properties for case B

In Case B, the arch dam was classified into eight sections. The properties of the dam components are shown in Table 6, and an illustration is provided in Fig. 15.

Table 6 Material properties of arch dam in case B

Arch dam part	Actual DEM (MPa)	Assumed damage index (d_e)	Measured DEM (MPa)
D1	36000	10%	32400
D2	34000	0%	34000
D3	37200	9%	33900
D4	37000	12%	32600
D5	41000	20%	32800
D6	33800	0%	33800
D7	40000	15%	34000
D8	38000	7%	35300

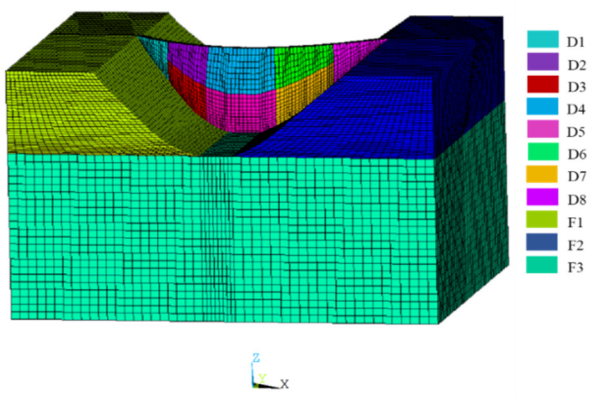

Fig. 15 Arch dam–foundation system for case B

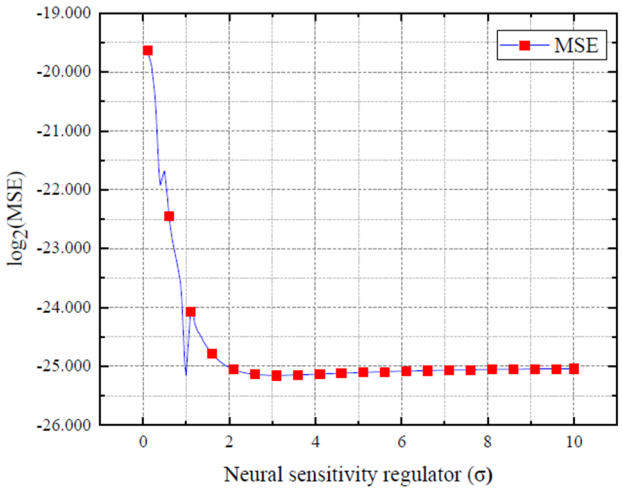

Fig. 17 The effect of neural sensitivity regulator i.e., σ on MSE for surrogate model in case B

5.4.2 Importance of sensor points selection

To efficiently identify the damage index and DEM parameters of the arch dam, we compared the two measurement point layout schemes shown in Fig. 16. Table 7 shows the final results for both schemes after noise was introduced using RBF and Jaya. As the identification accuracy of Scheme 2 was much higher than that of Scheme 1, the former was used for subsequent discussion.

5.4.3 Selection of neural sensitivity regulator component for case B

The neural sensitivity regulator component i.e., σ is selected equal to 1.0. The effect of σ on RBF based surrogate model is shown in Fig. 17, by calculation MSE.

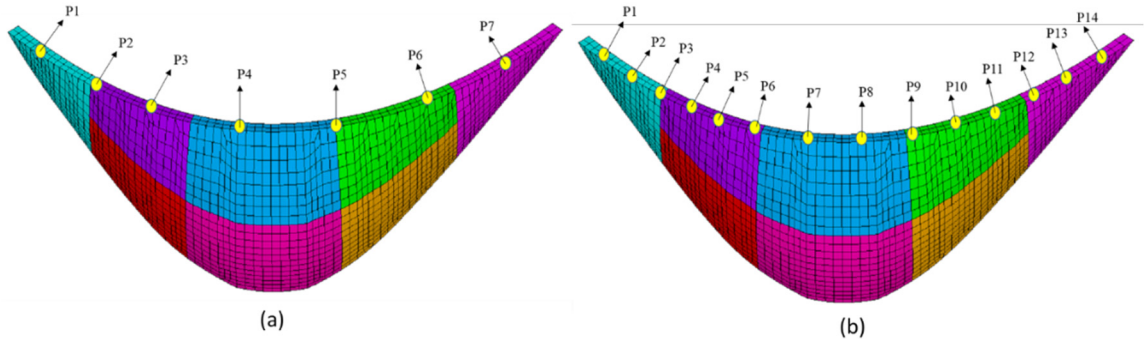

Fig. 16 Layout of measurement points for Case B: (a) Scheme 1: seven measurement points; (b) Scheme 2: fourteen measurement points

Table 7 Comparison results of two sensor layout schemes of measuring points with noise for Case B by RBF

Dam parameter	Measured DEM (MPa)	Scheme 1		Scheme 2	
		With Noise	Rel. error (%)	With Noise	Rel. error (%)
D1	32400	34170.499	5.465	32457.421	0.177
D2	34000	38588.725	13.496	37748.784	11.026
D3	33852	35135.097	3.790	35023.060	3.459
D4	32560	35336.009	8.526	33898.027	4.109
D5	32800	34231.119	4.363	31689.401	3.386
D6	33800	34656.207	2.501	35609.336	5.353
D7	34000	34960.529	2.825	34738.929	2.173
D8	35340	42346.686	19.827	39232.929	11.016
Average of errors (%)			**7.599**		**5.087**
Time for 30 runs (s)		168.325		171.740	**178.368**

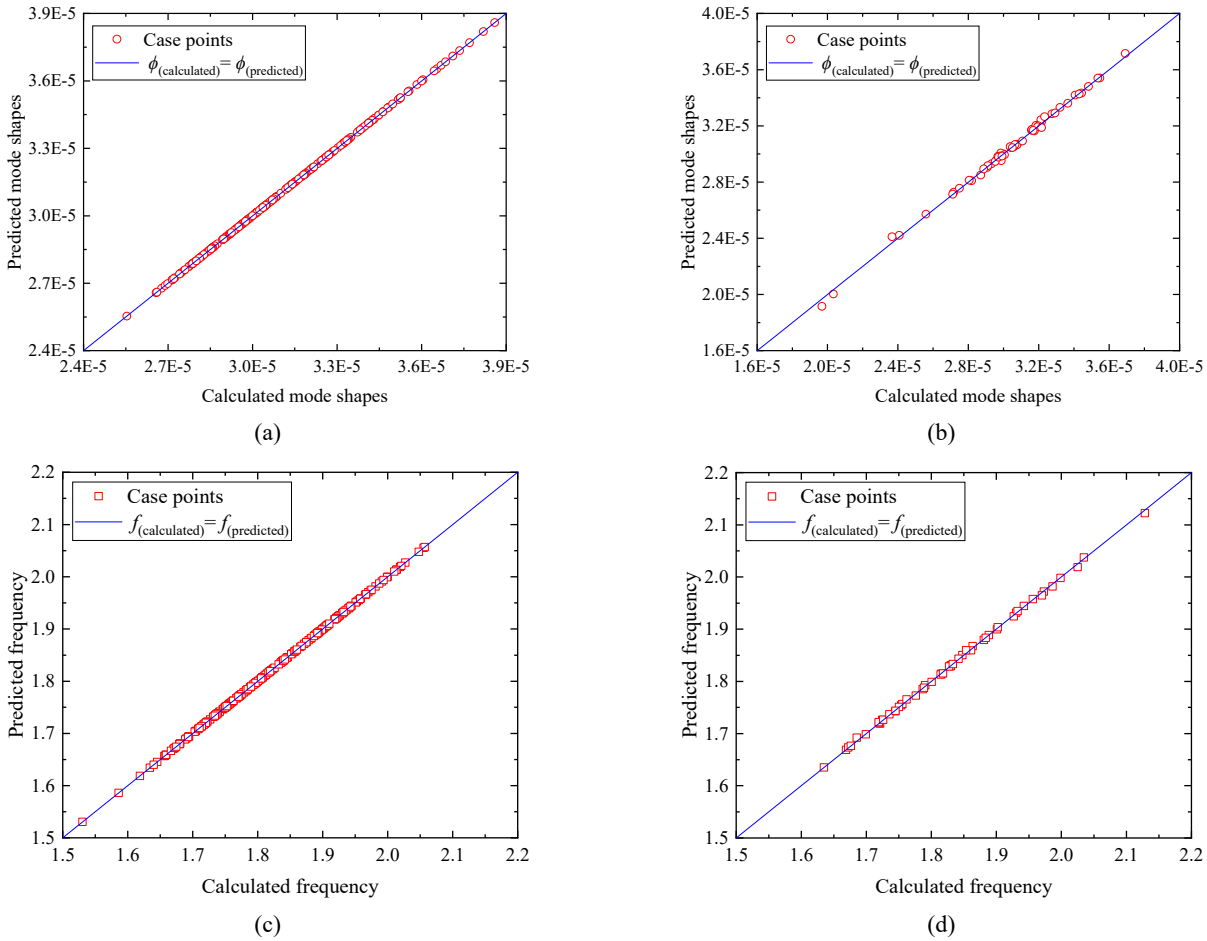

Fig. 18 Comparison between modal parameters calculated using FEM and predicted by RBF model in Case B for mode shapes and frequencies: (a), (b) Training datasets; (c), (d) Test datasets

Table 8 Fitting accuracy of RBF-based surrogate model in Case B

Data type	Natural frequency			Mode shapes		
	MAE	RMSE	R	MAE	RMSE	R
Training data	2.44E-15	3.12E-15	1.000	1.04E-18	2.95E-18	1.000
Test data	5.43E-03	8.56E-03	0.999	2.67E-06	7.72E-06	0.9651

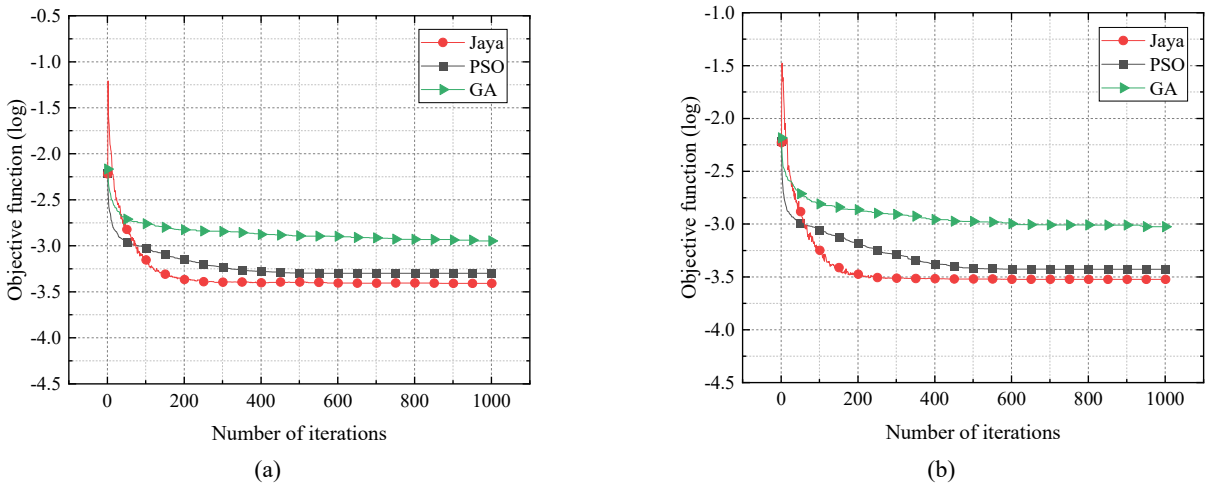

Fig. 19 Convergence process of objective function value of four algorithms in Case B using RBF model: (a) without noise; (b) with noise

5.4.4 RBF based surrogate model for case B

Fig. 18 shows the correlation between mode shapes and frequencies calculated with the FEM and predicted by the RBF model. As can be seen, all sample points were distributed near the diagonal, implying that the RBF model's vibration responses were close to the FE results. The RBF model's fitting accuracy is listed in Table 8.

5.4.5 Damage identification process by RBF for case B

Fig. 19 depicts the evolution of the objective function values for the four algorithms. The numerical values of the PSO algorithm and Jaya algorithm, converged at 5.03E-04 and 3.90E-04, respectively, whereas the numerical value of the GA algorithm converged at 1.13E-03, as shown in Fig. 19(a). The measured real frequencies and mode shapes were each subjected to 1% and 10% noise, respectively, to further confirm the fineness operation of the algorithms. Although noise was introduced, the PSO algorithm and Jaya algorithm, both converged at 3.74E-04 and 3.00E-04, respectively, whereas the GA provided the best solution at 9.44E-04, as shown in Fig. 19(b).

Fig. 20 (without noise) and Fig. 21 (with noise) show the identification process of the calculated damage indices d_2 and d_7 detected in dam parameters D2 and D7, respectively, for Case B. The values calculated using the Jaya for d_1, d_2, d_3, d_4, d_5, d_6, d_7, and d_8 were 11.301%, 9.617%, 9.32%, 9.822%, 24.521%, 4.51%, 17.623%, and 3.253%, respectively, which are similar to the assumed damage index, whereas those after noise were 9.84%, 11.626%, 5.852%, 8.384%, 22.709%, 5.353%, 13.153%, and 3.245%.

Eventually, in Fig. 22, the calculated damage index values for all parameters identified using the PSO algorithm, Jaya optimizer and GA, are compared to verify the accuracy of our technique, both with and without noise. Among all the damage detection algorithms, the Jaya produced the lowest average relative errors. The Jaya produced average errors of 3.6021% and 3.9816% for damage index identification with and without noise, respectively.

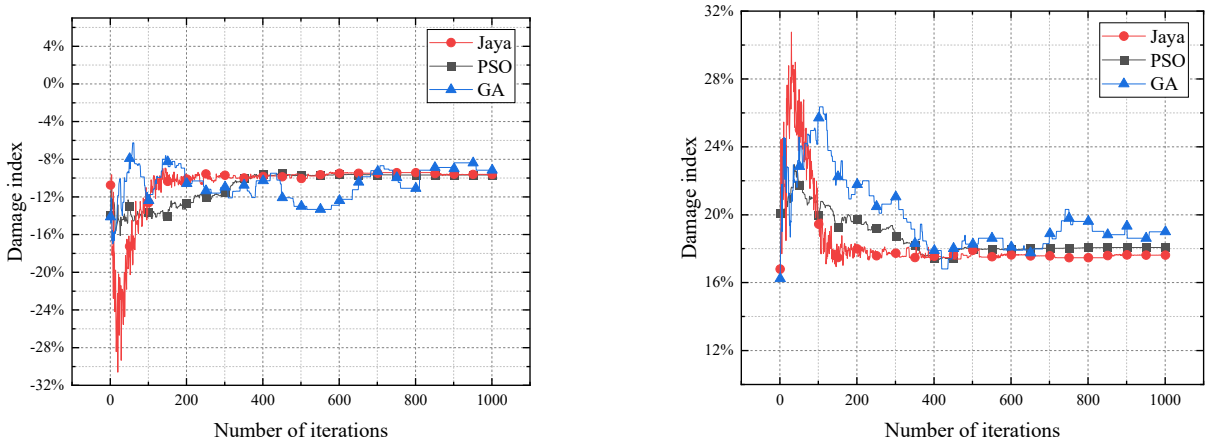

Fig. 20 Identification process of damage index of arch dam parameters without noise in Case B using RBF model: Damage index detected in (a) D2 and (b) D7

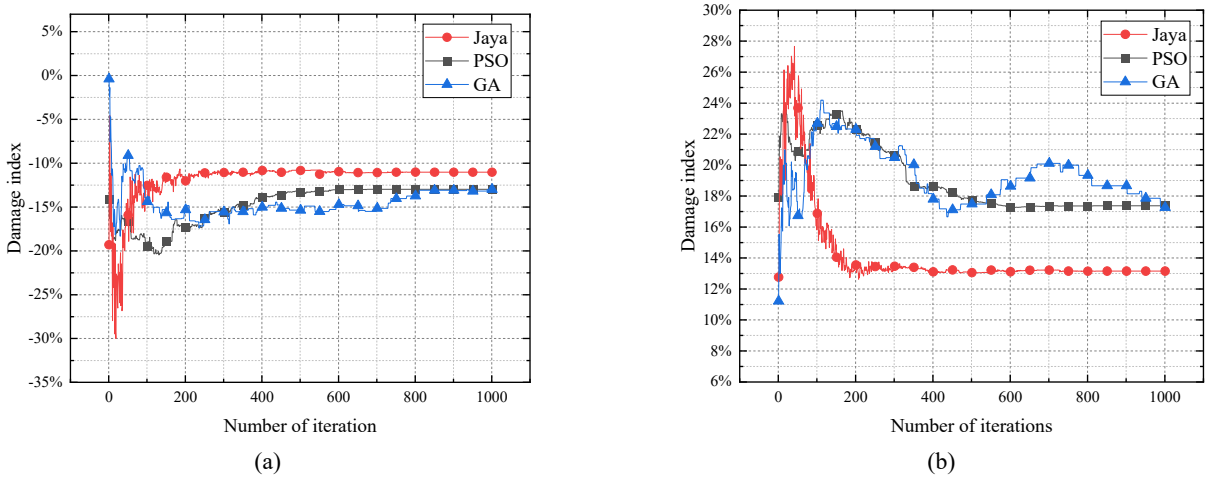

Fig. 21 Identification process of damage index of arch dam's parameters with noise in Case B using RBF model: Damage index detected in (a) D2 and (b) D7

Table 9 Comparison of measured and calculated DEM of arch dam without noise for Case B with the RBF-based surrogate model

Arch dam part	Measured DEM (MPa)	Jaya		PSO		GA	
		Calculated value (MPa)	Relative error (%)	Calculated value (MPa)	Relative error (%)	Calculated value (MPa)	Relative error (%)
D1	32400	31931.745	1.445	33145.794	2.302	33321.046	2.843
D2	34000	37269.842	9.617	37290.494	9.678	37113.239	9.157
D3	33852	33733.076	0.351	33208.710	1.900	33166.786	2.024
D4	32560	33365.840	2.475	33751.005	3.658	33301.478	2.277
D5	32800	30946.294	5.652	32385.632	1.263	32393.113	1.241
D6	33800	35324.344	4.510	35739.327	5.738	36043.705	6.638
D7	34000	32950.949	3.085	32772.462	3.610	32401.275	4.702
D8	35340	39236.205	11.025	38975.970	10.289	39837.274	12.726
Average of errors (%)			**4.770**		**4.805**		**5.201**
Time for 30 runs (s)		**174.527**		**167.819**		**364.982**	

Table 10 Comparison of measured and calculated DEM of arch dam with noise for Case B with the RBF-based surrogate model

Arch dam part	Measured DEM (MPa)	Jaya		PSO		GA	
		Calculated value (MPa)	Relative error (%)	Calculated value (MPa)	Relative error (%)	Calculated value (MPa)	Relative error (%)
D1	32400	32457.421	0.177	34177.658	5.487	34535.774	6.592
D2	34000	37748.784	11.026	38409.450	12.969	38418.525	12.996
D3	33852	35023.060	3.459	34078.586	0.669	33978.246	0.373
D4	32560	33898.027	4.109	34819.099	6.938	34895.788	7.174
D5	32800	31689.401	3.386	30701.151	6.399	30453.576	7.154
D6	33800	35609.336	5.353	36745.442	8.714	35899.291	6.211
D7	34000	34738.929	2.173	33052.441	2.787	33094.859	2.662
D8	35340	39232.929	11.016	41826.308	18.354	42177.909	19.349
Average of errors (%)			**5.087**		**7.790**		**7.814**
Time for 30 runs (s)		**178.368**		**171.255**		**369.324**	

Table 11 Calculation time for surrogate models and FE model for damage detection of arch dam for case A

Model type	Time required to build sample sets (sec)	Time required to establish surrogate model (sec)	Average time required to run inversion algorithm one time (sec)	Total time (sec)
FE model	-	-	52643.725	52643.725
RBF surrogate model	6580.465	0.474	5.5897	6586.528

Table 12 Calculation time for surrogate models and FE model for damage detection of arch dam for case B

Model type	Time required to build sample sets (sec)	Time required to establish surrogate model (sec)	Average time required to run inversion algorithm one time (sec)	Total time (sec)
FE model	-	-	53991.173	53991.173
RBF surrogate model	10756.234	0.303	6.133	10762.670

5.4.6 DEM calculations by dynamic parameter inversion analysis for case B

Finally, a comparison of the measured and calculated DEMs of the arch dam without and with noise for Case B with those obtained using the RBF-based surrogate model in Case B is presented in Tables 9 and 10. To compare the accuracy of the results, the relative errors and their average values are presented. Additionally, the computing time is provided to compare the efficiencies of the four algorithms. The results of the cases with and without noise were reasonable, and the Jaya was faster and more accurate than the other algorithms. In terms of parameter identification, the performance of the GA was subpar, i.e., the average relative error of parameter identification was 4.8038% without noise and 5.2156% with noise.

5.5 Efficiency of surrogate models w.r.t FE model

In both case A and B, efficiency has been calculated in terms of time required to complete the process for damage detection of arch dam using proposed hybrid approaches and FE model. For Case A and B, the calculation time for FE model and surrogate models with Jaya is represented in Tables 11 and 12, respectively. Efficiency and accuracy of RBF surrogate models for both cases, while utilizing Jaya for dynamic parameter identification, are presented and compared in Figs. 23 and 24, respectively.

5.6 Parameter sensitivity analysis

The simulation results for the weight coefficient of the objective function can affect the results. The weights of the natural frequency and mode shape must be selected deliberately. Therefore, some combinations of weights (w_1, w_2), such as (0.1, 0.9), (0.2, 0.8), (0.5, 0.5), and (0.8, 0.2), were investigated to obtain the ideal performance. The average errors for the calculated damage index were adopted to evaluate the damage detection performance of the proposed technique in Cases A and B. To highlight the

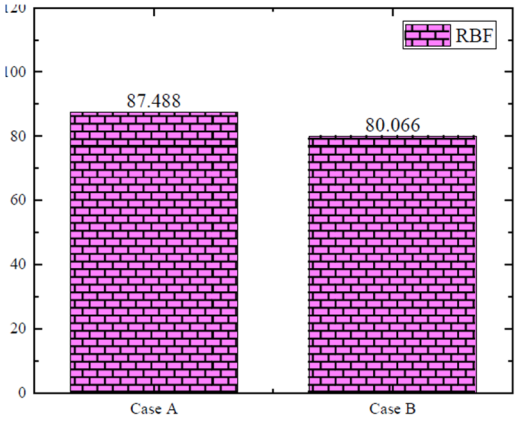

Fig. 23 Efficiency of RBF surrogate models (compared to FEM) with noise

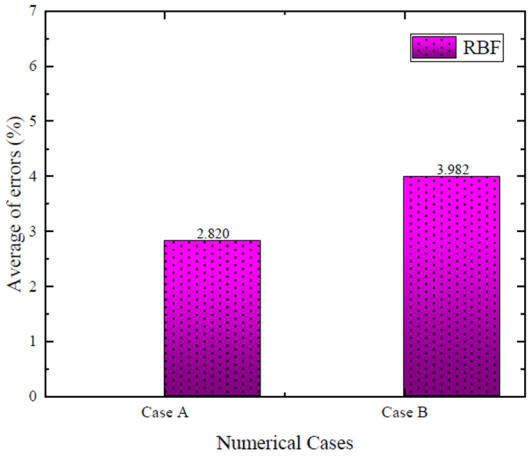

Fig. 24 Average of errors for DEM identification with RBF surrogate models with noise results

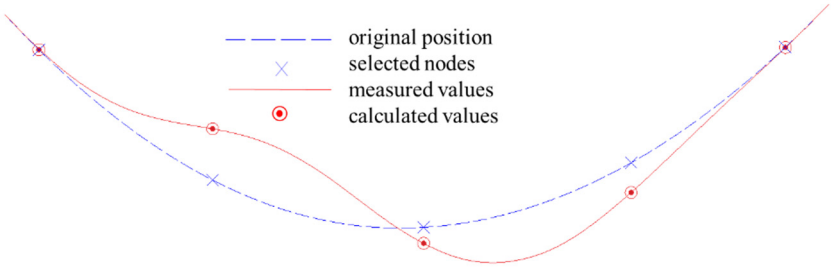

Fig. 25 Comparison between calculated and measured values of first-order mode shape at arch ring for Case A

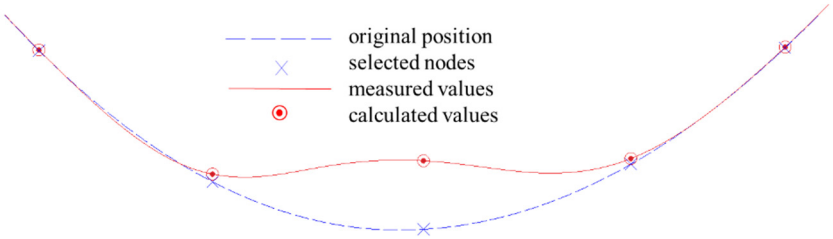

Fig. 26 Comparison between calculated and measured values of second-order mode shape at arch ring for Case A

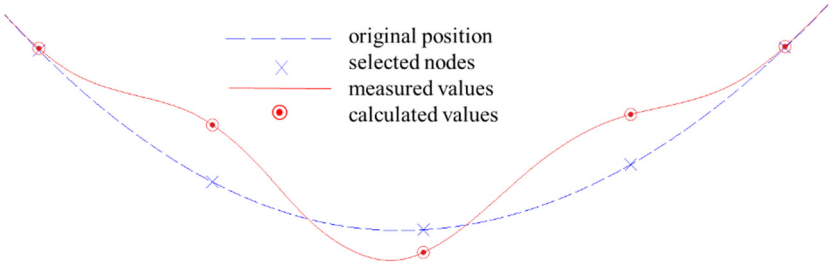

Fig. 27 Comparison between calculated and measured values of third-order mode shape at arch ring for Case A

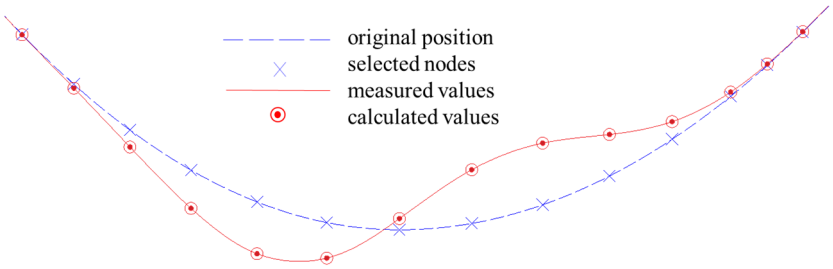

Fig. 28 Comparison between calculated and measured values of first-order mode shape at arch ring for Case B

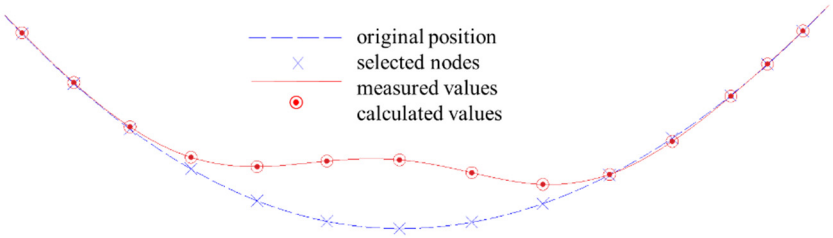

Fig. 29 Comparison between calculated and measured values of second-order mode shape at arch ring for Case B

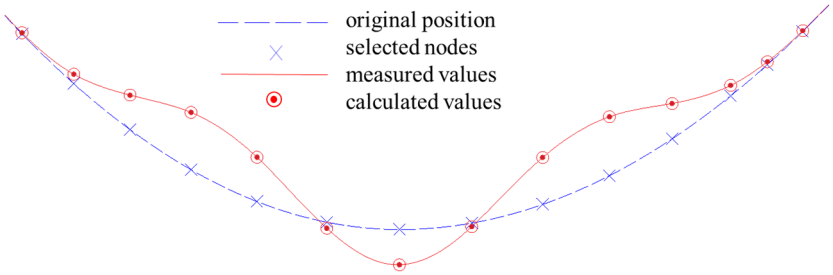

Fig. 30 Comparison between calculated and measured values of third-order mode shape at arch ring for Case B

noise was added to the measured natural frequencies and measured mode shapes, respectively. The effects of the weights shown in Eq. (6) on the performance of damage detection is presented in Table 13, and it appears that different combinations of weight coefficients did not significantly affect the inversion problem in this study. Hence, the combination of weights (w_1, w_2) was set as (0.5, 0.5) in both Cases A and B.

5.7 Model parameters calculation of arch dam

The measured and calculated frequencies along with the relative errors by using RBF surrogate model (with Jaya) are presented in Tables 14 and 15, for case A and B, respectively. The results shown in both Tables 14 and 15, are with noise results. Figs. 25-27 show a comparison between the first three measured and calculated mode shapes of the arch dam obtained using proposed hybrid model of RBF and Jaya with noise for Case A. Similarly, Figs. 28-30 show a comparison between the first three measured and calculated mode shapes of the arch dam obtained using proposed hybrid model of RBF and Jaya with noise for Case B.

Table 14 Comparison of calculated and measured frequencies using surrogate models with noise for Case A

Modal parameters	Measured value	RBF			
		Without noise		With noise	
		Calc. value	Rel. error (%)	Calc. value	Rel. error (%)
f_1	1.52794	1.53292	0.32592	1.54695	1.24415
f_2	1.76461	1.76512	0.02890	1.78313	1.04952
f_3	2.16532	2.16743	0.09744	2.19048	1.16195

Table 15 Comparison of calculated and measured frequencies using surrogate models with noise for Case B

Modal parameters	Measured value	RBF			
		Without noise		With noise	
		Calc. value	Rel. error (%)	Calc. value	Rel. error (%)
f_1	1.32221	1.32888	0.50445	1.34097	1.41883
f_2	1.42058	1.42803	0.52443	1.44108	1.44307
f_3	1.86645	1.87677	0.55292	1.89992	1.79324

6. Conclusions

In this study, a hybrid approach is proposed for determining the dynamic parameters of concrete arch dams using RBF-Neural Network surrogate models and Jaya algorithms. Latin Hypercube Sampling was utilized to acquire sample points for building the surrogate model. Jaya was used to optimize the objective function in the inverse analysis. The proposed method was tested on a hyperbolic concrete arch dam under various damage scenarios along with dynamic conditions, and the results were analyzed to reach the following conclusions.

- The proposed RBF model accurately depicts the connection between the dynamic elastic modolus (DEM) and modal parameters, using its strong machine learning capabilities. Compared to the Finite Element Method (FEM), the RBF-based surrogate model is much more computationally efficient.
- Compared to other machine learning and deep learning methods, the propsed novel hybrid approach use only one user defined parameter i.e NSR component that make it more generalizeable and reliable for real world problems.
- The novel Jaya algorithm proves to be effective in resolving the parameter identification problem. The results indicate that the Jaya optimizer offers improved speed and convergence accuracy compared to the PSO algorithm and Genetic algorithm.
- The proposed method for detecting damage to arch dams demonstrated encouraging results, making it suitable for calibrating finite element models and evaluating seismic performance in real-world applications with higher efficieny and accuracy.
- Furthermore, in future, we can make the damage indications on other phenomena like cracking or vertical joint opening in concrete arch dams or predicting dam behavior with other boundary conditions.

Acknowledgments

This research is jointly supported by the China Postdoctoral Science Foundation (No. 2018M631807), National Natural Science Foundation of China (Grant No. 51578202), Fundamental Research Funds for the Central Universities (Nos. N160103002, N170108029), National Natural Science Foundation of Liaoning (No. 201702281). The authors further acknowledge the support partially provided by USDOTs (693JK318500010CAAP and 693JK32110003POTA).

The results, discussion, and opinions reflected in this paper are those of the authors only and do not necessarily represent those of the sponsors. The research funds above are greatly appreciated by the authors. Author can provide training and test data sets for both Cases in case of intrusted reader or researchers request us.

References

Abbas, N., Yousaf, M., Akbar, M., Saeed, M.A., Huali, P. and Hussain, Z. (2022), "An experimental investigation and computer modeling of direct tension pullout test of reinforced concrete cylinder", **7**(3), p. 77.

Abbas, N., Umar, T., Salih, R., Akbar, M., Hussain, Z. and Haibei, X. (2023), "Structural Health Monitoring of Underground Metro Tunnel by Identifying Damage Using ANN Deep Learning", **13**(3), p. 1332. https://doi.org/10.3390/app13031332

Ahmed, S., Hussain, A., Hussain, Z., Pu, Z., Ostrowski, K.A. and Walczak, R. (2021), "Effect of carbon black and hybrid steel-polypropylene fiber on the mechanical and self-sensing characteristics of concrete considering different coarse aggregates' sizes", *Materials*, **14**(23), p. 7455. https://doi.org/10.3390/ma14237455

Alkayem, N.F., Cao, M., Zhang, Y., Bayat, M. and Su, Z. (2018), "Structural damage detection using finite element model updating with evolutionary algorithms: a survey", *Neural Comput. Applicat.*, **30**(2), 389-411. https://doi.org/10.1007/s00521-017-3284-1

Anitescu, C., Atroshchenko, E., Alajlan, N. and Rabczuk, T. (2019), "Artificial neural network methods for the solution of second order boundary value problems", *Comput. Mater. Continua*, **59**(1), 345-359. https://doi.org/10.32604/cmc.2019.06641

Bocciarelli, M. and Ranzi, G. (2018), "An inverse analysis approach for the identification of the hygro-thermo-chemical model parameters of concrete", *Int. J. Mech. Sci.*, **138**, 368-382. https://doi.org/10.1016/j.ijmecsci.2018.01.035

Chen, H.P. and Ni, Y.Q. (2018), "Vibration-Based Damage

Identification Methods", In: *Structural Health Monitoring of Large Civil Engineering Structures*, pp. 155-193. https://doi.org/10.1002/9781119166641.ch7

Chen, R., Li, J., Qian, Y., Peng, R., Jiang, S., Hu, C. and Zhao, Z. (2019), "An effective inverse procedure for identifying DEMparameters of rock-like materials", *Mathe. Probl. Eng.*, 2019. https://doi.org/10.1155/2019/6969546

Contursi, T., Messina, A. and Williams, E.J. (1998), "A multiple-damage location assurance criterion based on natural frequency changes", *J. Vib. Control*, **4**(5). 619-633. https://doi.org/10.1177/107754639800400505

Deng, W., Yao, R., Zhao, H., Yang, X. and Li, G. (2019), "A novel intelligent diagnosis method using optimal LS-SVM with improved PSO algorithm", *Soft Computing*, **23**, 2445-2462. https://doi.org/10.1007/s00500-017-2940-9

Dong, C.Z. and Catbas, F.N. (2021), "A review of computer vision–based structural health monitoring at local and global levels", *Struct. Health Monitor.*, **20**(2), 692-743. https://doi.org/10.1177/1475921720935585

Dou, S.Q., Li, J.J. and Kang, F. (2019), "Health diagnosis of concrete dams using hybrid FWA with RBF-based surrogate model", *Water Sci. Eng.,* **12**(3), 188-195. https://doi.org/10.1016/j.wse.2019.09.002

Goodfellow, I., Bengio, Y. and Courville, A. (2016), *Deep Learning*, MIT Press.

Hussain, Z., Pu, Z., Hussain, A., Ahmed, S., Shah, A.U., Ali, A. and Ali, A. (2021), "Effect of fiber dosage on water permeability using a newly designed apparatus and crack monitoring of steel fiber–reinforced concrete under direct tensile loading", *Struct. Health Monitor.*, **21**(5), 2083-2096. https://doi.org/10.1177/14759217211052855

Kang, F., Li, J.S. and Li, J.J. (2016), "System reliability analysis of slopes using least squares support vector machines with particle swarm optimization", *Neurocomputing*, **209**, 46-56. https://doi.org/10.1016/j.neucom.2015.11.122

Kang, F., Liu, J., Li, J. and Li, S. (2017), "Concrete dam deformation prediction model for health monitoring based on extreme learning machine", *Struct. Control Health Monitor.*, **24**(10), e1997. https://doi.org/10.1002/stc.1997

Kang, F., Wu, Y., Li, J. and Li, H. (2021), "Dynamic parameter inverse analysis of concrete dams based on Jaya algorithm with Gaussian processes surrogate model", *Adv. Eng. Inform.*, **49**, 101348. https://doi.org/10.1016/j.aei.2021.101348

Kaveh, A. and Laknejadi, K. (2013), "A new multi-swarm multi-objective optimization method for structural design", *Adv. Eng. Software*, **58**, 54-69. https://doi.org/10.1016/j.advengsoft.2013.01.004

Khatir, S., Belaidi, I., Khatir, T., Hamrani, A., Zhou, Y.L. and Wahab, M.A. (2017), "Multiple damage detection in composite beams using Particle Swarm Optimization and Genetic Algorithm", *Mechanics*, **23**(4), 514-521. https://doi.org/10.5755/j01.mech.23.4.15254

Kohiyama, M., Oka, K. and Yamashita, T. (2020), "Detection method of unlearned pattern using support vector machine in damage classification based on deep neural network", *Struct. Control Health Monitor.*, **27**(8), e2552. https://doi.org/10.1002/stc.2552

Le, V. and Caracoglia, L. (2020), "A neural network surrogate model for the performance assessment of a vertical structure subjected to non-stationary, tornadic wind loads", *Comput. Struct.*, **231**, 106208. https://doi.org/10.1016/j.compstruc.2020.106208

Lederman, G., Wang, Z., Bielak, J., Noh, H., Garrett, J.H., Chen, S., Kovacevic, J., Cerda, F. and Rizzo, P. (2014), "Damage quantification and localization algorithms for indirect SHM of bridges", *Proceedings of International Conference on Bridge Maintenance, Safety Management*, Shanghai, China, pp. 640-647. https://doi.org/10.13140/2.1.3308.8645

Lew, T.L., Spencer, A.B., Scarpa, F., Worden, K., Rutherford, A. and Hemez, F. (2006), "Identification of response surface models using genetic programming", *Mech. Syst. Signal Process.,* **20**(8), 1819-1831. https://doi.org/10.1016/j.ymssp.2005.12.003

Liu, K., Law, S.S. and Zhu, X.Q. (2017), "System parameter identification from projection of inverse analysis", *Journal of Sound and Vibration*, **396**, 83-107. https://doi.org/10.1016/j.jsv.2017.02.042

Majumdar, A., Maiti, D.K. and Maity, D. (2012), "Damage assessment of truss structures from changes in natural frequencies using ant colony optimization", *Appl. Mathe. Computat.*, **218**(19), 9759-9772. https://doi.org/10.1016/j.amc.2012.03.031

Mirjalili, S. (2023), The Genetic Algorithm (GA): Selection + Crossover + Mutation + Elitism, MATLAB Central File Exchange[CP]. Retrieved July 15, 2023

Nanthakumar, S.S., Lahmer, T., Zhuang, X., Zi, G. and Rabczuk, T. (2016), "Detection of material interfaces using a regularized level set method in piezoelectric structures", *Inverse Probl. Sci. Eng.*, **24**(1), 153-176. https://doi.org/10.1080/17415977.2015.1017485

Nguyen-Tuan, L., Koenke, C., Bettzieche, V. and Lahmer, T. (2018), "Uncertainty assessment in the results of inverse problems: applied to damage detection in masonry dams", *Int. J. Reliabil. Safety*, **12**(1-2), 2-23. https://doi.org/10.1504/IJRS.2018.092498

Nhamage, I.A., Lopez, R.H. and Miguel, L.F.F. (2016), "An improved hybrid optimization algorithm for vibration based-damage detection", *Adv. Eng. Software*, **93**, 47-64. https://doi.org/10.1016/j.advengsoft.2015.12.003

Olsson, A., Sandberg, G. and Dahlblom, O. (2003), "On Latin hypercube sampling for structural reliability analysis", *Struct. Safety*, **25**(1), 47-68. https://doi.org/10.1016/S0167-4730(02)00039-5

Pan, J., Xu, Y. and Jin, F. (2015), "Seismic performance assessment of arch dams using incremental nonlinear dynamic analysis", *Eur. J. Environ. Civil Eng.*, **19**(3), 305-326. https://doi.org/10.1080/19648189.2014.960950

Pandit, D., Zhang, L., Chattopadhyay, S., Lim, C.P. and Liu, C. (2018), "A scattering and repulsive swarm intelligence algorithm for solving global optimization problems", *Knowled.-Based Syst.*, **156**, 12-42. https://doi.org/10.1016/j.knosys.2018.05.002

Perera, R. and Ruiz, A. (2008), "A multistage FE updating procedure for damage identification in large-scale structures based on multiobjective evolutionary optimization", *Mech. Syst. Signal Process.*, **22**(4), 970-991. https://doi.org/10.1016/j.ymssp.2007.10.004

Rajasekaran, S. and Amalraj, R. (2002), "Predictions of design parameters in civil engineering problems using SLNN with a single hidden RBF neuron", *Computers & structures*, **80**(31), 2495-2505. https://doi.org/10.1016/S0045-7949(02)00213-4

Rao, R. (2016), "Jaya: A simple and new optimization algorithm for solving constrained and unconstrained optimization problems", *Int. J. Industr. Eng. Computat.*, **7**(1), 19-34. https://doi.org/10.5267/j.ijiec.2015.8.004

Rao, R.V. and More, K.C. (2017), "Design optimization and analysis of selected thermal devices using self-adaptive Jaya algorithm", *Energy Convers. Manage.*, **140**, 24-35. https://doi.org/10.1016/j.enconman.2017.02.068

Samaniego, E., Anitescu, C., Goswami, S., Nguyen-Thanh, V.M., Guo, H., Hamdia, K., Zhuang, X. and Rabczuk, T. (2020), "An energy approach to the solution of partial differential equations in computational mechanics via machine learning: Concepts, implementation and applications", *Comput. Methods Appl.*

Mech. Eng., **362**, 112790. https://doi.org/10.1016/j.cma.2019.112790

Stojanovic, B., Milivojevic, M., Ivanovic, M., Milivojevic, N. and Divac, D. (2013), "Adaptive system for dam behavior modeling based on linear regression and genetic algorithms", *Adv. Eng. Software*, **65**, 182-190. https://doi.org/10.1016/j.advengsoft.2013.06.019

Taheri, F., Ghasemi, M.R. and Dizangian, B. (2020), "Practical optimization of power transmission towers using the RBF-based ABC algorithm", *Struct. Eng. Mech., Int. J.*, **73**(4), 463-479. https://doi.org/10.12989/sem.2020.73.4.463

Teng, S., Chen, G., Yan, Z., Cheng, L. and Bassir, D. (2023), "Vibration-based structural damage detection using 1-D convolutional neural network and transfer learning", *Struct. Health Monitor.*, **22**(4), 2888-2909. https://doi.org/10.1177/14759217221137931

Trinh, M.C. and Jun, H. (2021), "Stochastic bending and buckling analysis of laminated composite plates using Latin hypercube sampling", *Eng. Comput.*, **39**(2), 1459-1497. https://doi.org/10.1007/s00366-021-01544-y

Tsihrintzis, G.A., Virvou, M., Sakkopoulos, E. and Jain, L.C. eds. (2019), *Machine Learning Paradigms*: *Applications of Learning and Analytics in Intelligent Systems*, Vol. 1, Springer. https://doi.org/10.1007/978-3-030-15628-2

Vorel, J. and Kabele, P. (2019), "Inverse analysis of traction-separation relationship based on sequentially linear approach", *Comput. Struct.*, **212**, 125-136. https://doi.org/10.1016/j.compstruc.2018.10.005

Wang, W., Kuang, Y., Li, S. and Ni, X. (2012), "Back analysis of dam parameter under seismic action", *Procedia Eng.*, **28**, 429-433. https://doi.org/10.1016/j.proeng.2012.01.745

Yang, L., Su, H. and Wen, Z. (2019), "Improved PLS and PSO methods-based back analysis for elastic modulus of dam", *Adv. Eng. Software*, **131**, 205-216. https://doi.org/10.1016/j.advengsoft.2019.02.005

Yuan, Q., Zhai, S., Wu, L., Chen, P., Zhou, Y. and Zuo, Q. (2019), "Blasting vibration velocity prediction based on least squares support vector machine with particle swarm optimization algorithm", *Geosyst. Eng.*, **22**(5), 279-288. https://doi.org/10.1080/12269328.2019.1607570

Zhang, A. and Zhang, L. (2004), "RBF neural networks for the prediction of building interference effects", *Comput. Struct.*, **82**(27), 2333-2339. https://doi.org/10.1016/j.compstruc.2004.05.014

Zhang, L., Wang, J.T., Xu, Y.J., He, C.H. and Zhang, C.H. (2020), "A procedure for 3D seismic simulation from rupture to structures by coupling SEM and FEM", *Bull. Seismol. Soc. Am.*, **110**(3), 1134-1148. https://doi.org/10.1785/0120190289

Notations

$\mathbf{K}$	Arch dam stiffness matrix
$\mathbf{M}_D$	Arch dam mass matrix
$\mathbf{M}_P$	Added mass matrix of arch dam elements (takes into account the dam's interaction with the reservoir in a dynamic manner)
ω_i	ith frequency
ϕ_i	mode shape (corresponds to ω_i)
M_i	The ith node's added mass, as calculated by Westergaard's formula
ρ_o	Density of reservoir water
M_i	Surface area of arch dam at node ith
H	water depth
h_i	Water surface distance from the ith node
k^e	intact stiffness matrices (eth element)
k_d^e	damaged stiffness matrices (eth element)
d_e	damage index (eth element)
f_i^m	using ith natural frequencies derived from undamaged structures in the FE model
f_i^c	calculated ith natural frequencies (FEM of damaged structure)
γ	frequency variation weighting factor
$\mathbf{E}$	a set of variables that required to be optimized
nf	frequencies count
ϕ_i^m	The modal components of ith mode shape (extracted from the FEM undamaged structure)
ϕ_i^c	The modal components of ith mode shape (extracted from the FEM damaged structure)
nm	mode shapes number
β	weighting factor for mode shape variation
n	count of measured modes
x	input layer neurons
g	premise function in the hidden layer process data from the input layer
y	final output from RBF neural network
c_j	a center vector with the same size as x
σ	neural sensitivity regulator component
$\|x - c_j\|^2$	the Euclidean distance between x and c_j
$\omega = (\omega_{jk})_{n\times p}$	network weight vector for output neurons
b	the output neurons' offset matrix
$f(\boldsymbol{u})$	the optimized objective function for Jaya algorithm
$\boldsymbol{u}_m$	a few solutions produced at random for Jaya algorithm (m is the population density)
$\boldsymbol{u}_{best}$	best solution analyses by $f(\boldsymbol{u})$
$\boldsymbol{u}_{worst}$	worst solution analyses by $f(\boldsymbol{u})$
$\mathbf{u}_{(j,k)}$	solution space' absolute value
$\boldsymbol{u}_{j,best}$	in the population, variable j represents the best member
$\boldsymbol{u}_{j,worst}$	in the population, variable j represents the worst member
$\boldsymbol{v}_{j,k}$	modified value for $\boldsymbol{u}_{j,k}$
$r_{1,j}$, $r_{2,j}$	arbitrary constants between [0, 1] in ith cycle for jth variable
y_{D_f}	simulated value for frequency
y_{Dm}	simulated value for mode shapes
y_f	individual measured values for frequency
y_m	individual measured values for mode shapes
N_f	set of observations for frequency
N_m	set of observations for mode shapes
MAE	mean absolute error
$RMSE$	root mean square error
R	correlation coefficient
y_D	individual calculated value
$\overline{y_D}$	average of the calculated values
y	individual values (measured quantities)
$\bar{y}$	average value (measured quantities)
N	the set of observations
F	foundation part of Arch dam foundation system
D	dam part of Arch dam foundation system